

An H_{α} Catalogue of Galaxies in Hickson Compact Groups. I. The Sample

P. Severgnini,^{1,4} B. Garilli¹, P. Saracco² and G. Chincarini^{2,3}

¹ IFCTR/CNR, Via Bassini, 15, 20133 Milano, Italy

² Osservatorio Astronomico di Brera-Merate, Milano, Italy

³ Dip. di Fisica, Univ. Milano, Via Celoria, 16, 20133 Milano, Italy

⁴ Univ. degli Studi di Firenze, Dip. Astronomia e Scienza dello Spazio, Via Fermi 5, 50125 Firenze (Arcetri), Italy.

email: paola@ifctr.mi.cnr.it; bianca@ifctr.mi.cnr.it; saracco@merate.mi.astro.it; guido@merate.mi.astro.it

Received; accepted

Abstract. We present H_{α} photometry for a sample of 95 galaxies in Hickson Compact Groups obtained from observations of 31 groups. The Catalogue lists isophotal and adaptive aperture (Kron aperture) flux measurements for about 75% of the accordant galaxies inside the observed HCGs, 22 out of which are upper limits. Non standard data reduction procedures have been used to obtain the continuum subtracted H_{α} images for each HCG of the target sample. Flux calibration has also been performed in order to obtain H_{α} luminosities for the whole sample. Both the data reduction and calibration procedures are carefully described in this paper. The new data listed in this Catalogue are of great importance in understanding the star formation rate inside HCG galaxies and in giving new insights on its dependence on galaxy interactions.

Key words: galaxies: groups; interaction; merger – H_{α} emission – star formation

1. Introduction

Hickson Compact Groups (hereafter HCGs; Hickson 1982; Hickson 1993) are small systems of several galaxies (four or more) in an apparent close proximity in the sky. The debate on their physical reality as bounded systems is still open. A possibility exists that only a part of the sample of HCGs are bound systems and/or that HCG dynamical evolution depends on their environments. Important informations about their real nature could be obtained by studying the rate of merger and interaction between their galaxies. The studies carried out so far agree with the view of a low merging rate inside HCGs with respect to undisrupted systems of galaxies (Zepf et al. 1991, Zepf 1993). On the other hand it is not so clear which is the fraction of interacting galaxies in HCGs: photometric and spectroscopic studies (Rubin et al. 1991; Mendes de Oliveira et al. 1997; Moles et al. 1994; Mendes de Oliveira et al.

1994; Vilchez & Iglesias Paramo 1998a; Vilchez & Iglesias Paramo 1998b; Iglesias Paramo & Vilchez 1999) have often given contradictory results. It is expected that interaction and merger phenomena strongly affect the star formation rate (*SFR*) of galaxies. In particular, interacting galaxies should show an higher star formation rate than field galaxies. Thus the study of star formation of galaxies in HCGs gives important clues about the interaction and merger phenomena inside them. Powerful tools to investigate on the star formation activity are the ionization lines emitted by the heated gas surrounding the regions of star formation. The H_{α} emission line at 6563 Å can be used as a quantitative and spatial tracer of the rate of massive ($\geq 10 M_{\odot}$) and therefore recent ($\leq 10^7$ years) star formation (Kennicutt 1983; Ryder & Dopita 1994), unlike the color indexes in the U, B, V filters, that give indications about the past star formation ($> 10^8$ years). Therefore, by knowing the H_{α} emission of the HCG galaxies it is possible in principle to carry out important investigations about the present merger and interaction events in these systems. Up to now, only Rubin et al. (1991) and more recently Vilchez & Iglesias Paramo (1998a) have collected significant samples of H_{α} data on HCG galaxies. They published H_{α} emission-line images respectively for 14 and 16 HCGs. While Vilchez & Iglesias Paramo (1998a) estimate the H_{α} flux for each of the 63 galaxies of their sample, Rubin et al. do not use flux calibrated and they take into account a sample constituted by disk galaxies only. H_{α} data for the galaxies of single groups have been also obtained by Valluri & Anupama (1992), Mendes de Oliveira et al. (1994) and Plana et al. (1998). Valluri & Anupama presented H_{α} calibrated data for the galaxies of HCG62 and Mendes de Oliveira et al. and Plana et al. reported kinematic observations of H_{α} emission respectively for four late-type galaxies of HCG16 and for two early-type galaxies and one disk system of HCG90.

With the aim to obtain quantitative informations about the H_{α} emission of HCGs galaxies we have observed 31 HCG in narrow-band interferometric filters deriving H_{α}

calibrated fluxes for 95 galaxies, 22 out of which are upper limits. In this paper we present the catalogue containing these H_{α} data.

We first describe the sample and the observations in § 2 and in § 3. In § 4 and § 5 we present the data reduction and calibration procedures used. The Zero Point correction, Galactic and Internal extinction corrections applied to the fluxes are described in § 6, while § 7 contains the photometric error derivation. In § 8 we present the H_{α} Catalogue of Galaxies, while in § 9 we derive the star formation rate for the whole sample. Finally we briefly discuss some of the observed groups in § 10.

2. The Sample

The 100 compact groups catalogue by Hickson (1982) has been revised by Hickson, Kindl & Auman (1989) and then by Hickson et al. (1992). By adding a radial velocity criterion Hickson et al. (1992) were able to reject probable non member galaxies. The resulting sample consists of 92 groups each containing three or more "accordant" members, which have radial velocities differing by no more than 1000 km s^{-1} from the median velocity of the group. Our sample has been drawn from this latest catalog.

In this paper, the result of the data reduction and calibration of H_{α} CCD images are presented for 31 Hickson Compact Groups. The remaining 61 HCGs were not in our sample because the adequate H_{α} interferometric filters were not available during the observations. This is the only criterion used to select the observed groups.

The redshift of observed groups is in the range $0.005 \leq z \leq 0.07$ (P. Hickson et al., 1992) and their distribution is shown in Figure 1 (the width of each bin is 0.01).

Table 1 lists the observed HCGs as follows:

Col.1: Name of the groups according to Hickson's catalogue;
 Col.2: 1950 right ascension (R.A.) of the centroid of the member galaxies;
 Col.3: 1950 declination (Dec.) of the centroid of the member galaxies;
 Col.4: Number of accordant members of the group;
 Col.5: Velocity dispersion of the group: $\sigma_v (\text{Km s}^{-1})$;
 Col.6: Mean Redshift of the group.

The sample is composed by 134 galaxies, 127 out of which have been observed. 52% of them are Ellipticals and Lenticulars and the remaining 48% are Spirals and Irregulars. For each observed galaxy we report in Table 2 the heliocentric radial velocity V in units of Km s^{-1} , the total magnitude in the photographic band B_T , corrected for internal and galactic extinction and the Hubble type, as in Hickson 1993. Galaxies are named with the number of HCG plus letter of galaxy itself.

The distribution of the total B_T magnitude of the observed galaxies is shown in Figure 2 (the width of each bin is 0.5 magnitude).

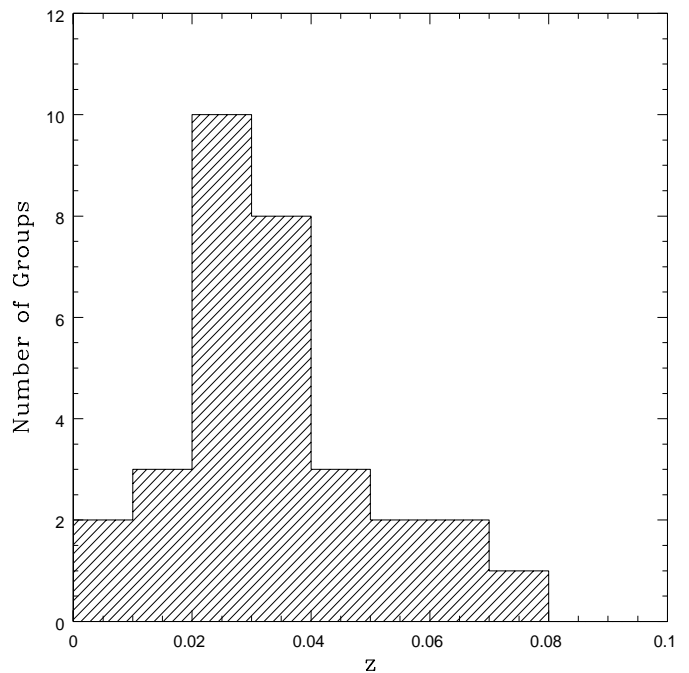


Figure 1: Redshift distribution of the 31 observed groups.

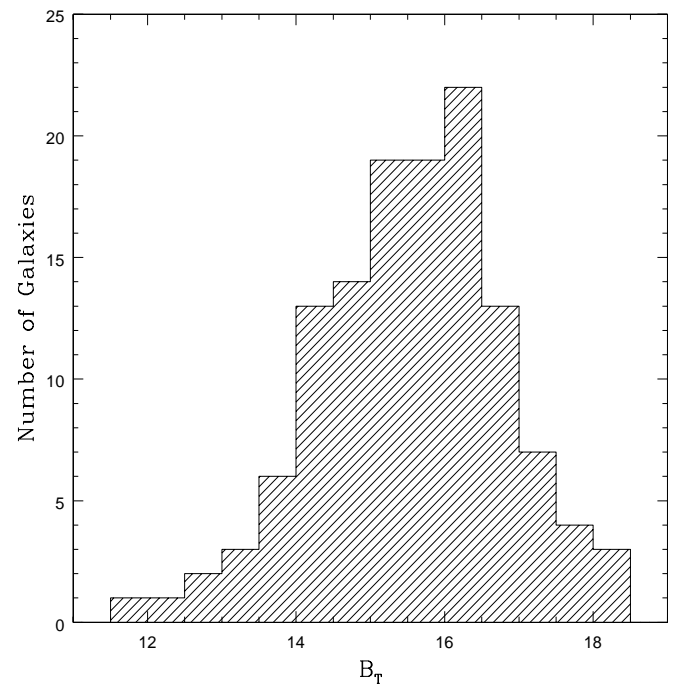


Figure 2: Distribution of B_T magnitude of the 127 observed galaxies.

3. Observations

The CCD images of the HCG sample were obtained during three different observing runs (November 1995, April 1996 and February 1997).

Table 1: Observed Hickson Compact Groups (Hickson et al., 1992): HCG number, right ascension and declination (1950), number of accordant galaxies, velocity dispersion and mean redshift of group.

HCG	R.A. (1950)	Dec. (1950)	N°	σ_v ($\frac{Km}{s}$)	z
2	0 28 48.97	8 10 19.3	3	54.9	0.0144
15	2 5 2.95	1 54 58	6	426.6	0.0228
33	5 7 53.69	17 57 51	4	154.9	0.026
34	5 19 6.72	6 38 5.7	4	316.2	0.0307
35	8 41 56.87	44 42 16.4	6	316.2	0.0542
37	9 10 35.78	30 12 58	5	398.1	0.0223
38	9 24 58.06	12 29 58.4	3	12.9	0.0292
43	10 8 39.7	0 11 32.7	5	223.9	0.033
45	10 15 46.72	59 21 27.8	3	182.0	0.0732
46	10 19 29.69	18 6 39.5	4	323.6	0.027
47	10 23 7.57	13 59 28.2	4	42.6	0.0317
49	10 53 19.24	67 26 54.2	4	33.9	0.0332
53	11 26 18.96	21 2 13.9	3	81.3	0.0206
54	11 26 38.24	20 51 38.4	4	112.2	0.0049
56	11 29 53.51	53 13 16.5	5	169.8	0.027
59	11 45 53.12	12 59 51.3	4	190.5	0.0135
66	13 36 47.14	57 33 45.5	4	302	0.0699
68	13 51 29.15	40 33 26.9	5	154.9	0.008
69	13 53 12.58	25 18 44	4	223.9	0.0294
70	14 1 54.07	33 34 13.7	4	144.5	0.0636
71	14 8 45.02	25 44 4.1	3	416.8	0.0301
72	14 45 36.94	19 16 2.6	4	263	0.0421
74	15 17 12.89	21 4 31.9	5	316.2	0.0399
75	15 19 19.7	21 21 45.3	6	295.1	0.0416
76	15 29 14.96	7 29 20.1	7	245.5	0.034
79	15 56 59.93	20 53 51	4	130.0	0.0145
81	16 15 54.25	12 54 57.6	4	177.8	0.0499
82	16 26 28.03	32 56 21	4	616.6	0.0362
83	16 33 12.91	6 22 9.6	5	457.1	0.0531
92	22 33 40.37	33 42 12.6	4	389.0	0.0215
96	23 25 28.19	8 29 55.4	4	131.8	0.0292

Observations have been carried out at the 2.1 meter telescope (design Ritchey-Chretien) at the National Observatory of Mexico in S. Pedro Martir (SPM). The SPM Cassegrain focus ($f/7.5$) was coupled with a Tektronix CCD of 1024x1024 pixels, each $24\mu m \times 24\mu m$. The telescope scale (13 arcsec/mm) and the pixel dimensions provide a pixel size of 0.3 arcsec/pix with a resulting field of view of $5.12' \times 5.12'$. The CCD gain is $4 e^-/\text{ADU}$.

During these three runs we observed 31 HCGs. All images were obtained with seeing conditions in the range 2-2.6 arcsec. For each HCG two CCD images were taken: the *on image*, by using a narrow-band interference filter (H_{α}^{on} filter) centered on the wavelength of the H_{α} line redshifted to the z of the galaxy (which isolates the H_{α} emission-line and underlying continuum), and the *off image*, by using another interference filter (H_{α}^{off} filter) of similar bandwidth but centered on an adjacent region of the spectrum (isolating continuum light only). Table 3 describes the fea-

tures of narrow band filters used in this work. In the third column the range of recession velocity that a galaxy should have to give out its H_{α} line through the interferential filter is shown.

In order to calibrate our data, we have observed some

Table 3: Features of interferometric filters: central wavelength, FWHM and corresponding velocity interval

$\lambda_{central}$ (\AA)	FWHM (\AA)	Velocity Interval ($Km s^{-1}$)
6546	81	-2628 \rightarrow 1074
6564	72	-1600 \rightarrow 1691
6603	80	0 \rightarrow 3657
6607	89	-23 \rightarrow 4045
6641	79	1760 \rightarrow 5371
6643	80	1828 \rightarrow 5485
6683	80	3657 \rightarrow 7314
6690	91	3725 \rightarrow 7885
6723	80	5485 \rightarrow 9142
6732	74	6034 \rightarrow 9416
6742	85	6240 \rightarrow 10216
6819	86	9736 \rightarrow 13668
6920	88	1431 \rightarrow 18330
7027	93	1908 \rightarrow 23335

spectrophotometric stars, equally spaced in time during each night, from the list of Massey & Strobel (1988). Table 4 lists the standards used. The spectrophotometric standards were observed in the same H_{α} narrow-band interference filters used to observe Hickson Compact Groups.

Table 4: Standard stars used for calibration

Star	α_{1950} ($h m s$)	δ_{1950} ($^{\circ} ' ''$)
PG0205+134	02 05 21.3	+13 22 18
Hiltner 600	06 42 37.2	+02 11 25
PG0939+262	09 39 58.8	+26 14 42
Feige34	10 36 41.2	+43 21 50
PG1121+145	11 21 39.4	+14 30 18
Feige66	12 34 54.7	+25 20 31
Feige67	12 39 18.9	+17 47 24
Kopf27	17 41 28	+05 26 04

The flux from $[N_{II}]$ emission lines ($\lambda=6548 \text{ \AA}$ and $\lambda=6584 \text{ \AA}$) is included in the on observations. Therefore the flux and luminosity here estimated refer to the sum of H_{α} and $[N_{II}]$ emission lines and not only to H_{α} . Nevertheless through this paper we refer for simplicity to them as $f_{H_{\alpha}}$ and $L_{H_{\alpha}}$ respectively. The aim of the observations was to study the recent star formation rate occurring in HCG galaxies. Since the $H_{\alpha} + [N_{II}]$ emission a good star formation tracer as well as the H_{α} line alone (Kennicutt &

Ken, 1983), the presence of $[N_{II}]$ does not invalidate our data. Nevertheless, since the $H_{\alpha}/[N_{II}]$ ratio is not constant with radius in the largest galaxies, we will refer to the global star formation rate of galaxies, that is to the rate integrated over all the emitting area of each galaxy.

In Table 5 the journal of the observations is reported as follows:

Col.1: Name of the groups;
 Col.2: Observing date (mm-yy);
 Col.3: Central wavelength for the H_{α}^{on} filter used (\AA);
 Col.4: Integration time for H_{α}^{on} filter exposure (s);
 Col.5: Central wavelength for the H_{α}^{off} filter used (\AA);
 Col.6: Integration time for H_{α}^{off} filter exposure (s).

Table 5: Journal of observations

Group	Date (mm-yy)	H_{α}^{on} \AA	T_{exp} (s)	H_{α}^{off} \AA	T_{exp} (s)
HCG2	Nov.95	6643	1800	6723	1800
HCG15	Nov.95	6723	1800	6643	1800
HCG33	Nov.95	6723	1800	6643	1800
HCG34	Feb.97	6732	1800	6564	1800
HCG35	Feb.97	6920	1800	6690	1800
HCG37	Nov.95	6723	1800	6643	1800
HCG38	Nov.95	6723	1800	6643	1800
HCG43	Feb.97	6819	1800	6607	1800
HCG45	Feb.97	7027	1800	6819	1800
HCG46	Nov.95	6723	1800	6643	1800
HCG47	Apr.96	6732	1800	6564	1800
HCG49	Apr.96	6819	1800	6690	1800
HCG53	Apr.96	6690	1800	6607	1800
HCG54	Nov.95	6603	1200	6683	1200
HCG56	Apr.96	6732	1800	6564	1800
HCG59	Apr.96	6690	1800	6607	1800
HCG66	Apr.96	7027	1800	6920	1800
HCG68	Feb.97	6607	1200	6819	1200
HCG69	Apr.96	6732	1800	6564	1800
HCG70	Apr.96	7027	1800	6920	1800
HCG71	Feb.97	6732	1800	6564	1800
HCG72	Apr.96	6819	1800	6690	1800
HCG74	Feb.97	6819	1800	6607	1800
HCG75	Apr.96	6819	1800	6690	1800
HCG76	Apr.96	6819	1800	6690	1800
HCG79	Apr.96	6690	1800	6607	1800
HCG81	Apr.96	6920	1800	6819	1800
HCG82	Apr.96	6819	1800	6920	1800
HCG83	Apr.96	6920	1800	6819	1800
HCG92	Nov.95	6723	1800	6643	1800
HCG96	Nov.95	6723	1800	6643	1800

4. Data Reduction

4.1. Bias and Flat-Field Corrections

The science frames have been first bias subtracted. For each observing run, we have obtained the proper bias

by combining several bias frames with a median filter. Then the images have been corrected for pixel to pixel response variations. For each night, its own flat field has been constructed by medianing several flat field frames carried out during the night.

Two different types of flat fields have been used during the three observing runs: the first one has been obtained by medianing twilight sky images and it has been used to reduce the data of 1996. The other one, used in 1995 and 1997 runs, has been constructed by medianing flat field frames taken on the dome illuminated with twilight sky. No significant differences have been measured by using the two flat fields.

These two steps of data reduction are based on the NOAO IRAF package, developed at the Center for Astrophysics. Finally, cosmic rays and bad pixels have been removed from each frame using Munich Image Data Analysis System (MIDAS).

4.2. H_{α} Emission-Line Map

The map of the H_{α} emission-line flux for each HCG (H_{α} image) has been obtained by removing the contribution of the underlying continuum, that is by subtracting the H_{α}^{off} from the H_{α}^{on} (Pogge, 1992). There are several reasons why the number of continuum photons per integration time unit passing through the *on filter* can be different from the one through the *off filter*. For example differences between the transmission curves of the two narrow-band filters, such as different width and/or transmission peak; or variations of the sky transparency during the night. This implies that in order to obtain the H_{α} emission-line flux image a careful estimation of the underlying continuum to subtract from the H_{α}^{on} is required. In practice, the H_{α}^{off} have to be rescaled to the continuum of the H_{α}^{on} wavelength. Since stars do not show H_{α} emission, the number of continuum photons coming from the stars in each HCG field and passing through the *on* and *off* filters have to be the same. In-fact, although the *on* and *off* filters are sometimes separated by more than 150 \AA , implying that the number of photons coming from the stars is not rigorously the same, such a difference is negligible. Thus for each HCG field (and for each couple of filters) we have selected at least three stars and we have calculated the mean scaling factor K

$$K = \frac{1}{N} \sum_{i=1}^N \left(\frac{C_{on}}{C_{off}} \right)_i = \left\langle \left(\frac{C_{on}}{C_{off}} \right) \right\rangle \quad (1)$$

where C_{on} and C_{off} are the counts from stars in the *on* and *off* image respectively, and N is the number of stars. Once rescaled, the H_{α}^{off} have been spatially aligned to the H_{α}^{on} . The alignment has been performed by applying the IRAF tasks *geomap/geotran* using the position of at least five stars in the field as reference coordinates. Finally, after

having additively rescaled the *on* and *off* images to the same median value, we have subtracted the H_{α}^{off} from the H_{α}^{on} thus obtaining the image of the H_{α} emission-line flux.

5. Photometric Calibration

We have measured instrumental magnitudes of standard stars by constructing for each star its growth curve through circular concentric apertures. The magnitude has been taken at the convergence of the curve. From the spectral energy distributions of our observed standard stars (Massey & Strobel 1988), we have derived their apparent magnitudes at the effective wavelengths λ_{eff} of our filters, through the usual relation

$$m_{vF} = -2.5 \cdot \log_{10} f_{\lambda_{eff}}(m_{vF}) + 2.5 \log_{10} f_{\lambda_{eff}}(0) \quad (2)$$

where F is a generic filter, $f_{\lambda_{eff}}(m_{vF})$ and $f_{\lambda_{eff}}(0)$ are the spectral irradiances in $\text{erg cm}^{-2} \text{ s}^{-1} \text{ \AA}^{-1}$ within the F filter having the effective wavelength $\lambda_{eff}(F)$ of a star of magnitude m_{vF} and of a star of $m_{vF}=0$ respectively. From each star we have derived the zero point Z_p of the photometric calibration for the different filters and nights.

The standard deviation of the zero point values thus obtained is within 0.05 mag during all but one night. During this night the scatter is much larger than a factor of four. Thus with the aim at maintaining the uncertainty on the galaxy photometry within few hundreds percent, we have considered only those galaxies observed during photometric nights, i.e. those nights for which $\sigma_{Z_p} \leq 0.05$ mag.

6. The H_{α} Emission of Galaxies

6.1. Instrumental H_{α} Fluxes

Following the data reduction steps described in section §4, we have obtained 31 emission-line images, one for each HCG of our sample. We have computed both isophotal and adaptive-aperture H_{α} fluxes for the HCG galaxies in the 31 fields by using SExtractor (Bertin et al. 1996). The full analysis of each image is divided in six steps: sky background estimation, thresholding, deblending, filtering of the detections, photometry and star/galaxy separation. For each continuum-subtracted H_{α} image we have used a detection threshold of one sigma above the background. The H_{α} isophotal fluxes have been computed within the region defined by the detection threshold. In addition to the isophotal flux we have also considered the corrected isophotal flux estimated by SExtractor that should take into account the fraction of flux lost by the isophotal one (Bertin et al. 1996). In addition the adaptive-aperture photometry has also been calculated (Kron 1980; Bertin et al. 1996).

Out of the 127 accordant observed galaxies belonging to the 31 HCG of our sample, we have been able to compute isophotal and adaptive-aperture photometry for 73 and

69 galaxies respectively. The 1σ limiting flux, integrated within the mean seeing disk (2.3 arcsec), reached in our observations ranges between $1.43 \cdot 10^{-16}$ and $4.13 \cdot 10^{-17} \text{ erg cm}^{-2} \text{ s}^{-1}$.

For 22 galaxies, which have not been detected in our H_{α} images, we have computed the 3σ upper limits above the background:

$$f_{ul} = 3 \cdot rms \cdot \left[\left(\frac{FWHM}{2} \right)^2 \cdot \pi \right]^{\frac{1}{2}} \quad (3)$$

being

$$\begin{aligned} rms & \quad \text{the sky estimation accuracy} \\ & \quad (\text{counts pix}^{-1} \text{ s}^{-1}); \\ \left[\left(\frac{FWHM}{2} \right)^2 \cdot \pi \right]^{\frac{1}{2}} & \quad \text{the squareroot of the seeing area in} \\ & \quad \text{pixels.} \end{aligned}$$

For the remaining 32 galaxies we have not been able to estimate the H_{α} fluxes because of one of the following reasons:

1. the night was not photometric ($\sigma_{Z_p} >> 0.05$ mag);
2. the proper narrow band interference filter was not available;
3. too much imperfections are present on the H_{α} image probably due to large variations in seeing conditions between the *on* and *off* band exposures, or due to changes in the telescope focus (e.g. because of substantially different thickness of the filters and/or temperature variations).

In Table 6 we list the galaxies for which it was not possible to measure their flux and the corresponding reason (1,2,3).

6.2. Zero Point Correction

In order to obtain calibrated fluxes and luminosities for our sample of galaxies, we have estimated the zero point flux correction, Z_{flux} such that

$$f_{H_{\alpha}} = (f_{on} - f_{off}) = Z_{flux} \cdot [C_{on} - C_{off}] \quad (4)$$

where:

f_{on}, f_{off} are the isophotal or aperture H_{α} fluxes of galaxy in the *on* and the scaled *off* filters respectively;

C_{on}, C_{off} are the counts of the galaxy in the *on* and *off* band images respectively;

It can be proved that the Z_{flux} coefficient of each galaxy is proportional to $Z_{flux_{on}}$ i.e. the zero point flux correction of the *on* band image. Knowing the $Z_{flux_{on}}$ in magnitudes ($Z_{p_{on}}$, see §5) and the extinction coefficient k_{on} of the site relative to each filter, we have derived the correction factor $Z_{flux_{on}}$ as follows:

$$Z_{flux_{on}} = \Delta \lambda \cdot 10^{-0.4(Z_{p_{on}} - (k_{on} \cdot X_s) - b)} \quad (5)$$

where X_s is the airmass of the standard star and b is

$$b = 2.5 \cdot \log_{10} f_{\lambda_{eff}}(0) \quad (6)$$

Thus Z_{flux} is given by

$$Z_{flux} = \frac{Z_{flux_{on}}}{10^{-0.4(k_{on} \cdot X_g)}} \cdot 10^{[0.4(k_{on} \cdot X_g)]} \quad (7)$$

where X_g is the airmass of the target galaxy. This zero point correction was applied to the H_{α} instrumental fluxes and to the upper limits estimated for the undetected galaxies. Fluxes and upper limits have been also corrected so that the H_{α} emission-line of the galaxy passes exactly in the center of the corresponding *on* filter band, i.e. for the percentage of total flux lost if the H_{α} emission line of the galaxy does not pass exactly in the center of the corresponding *on* filter. The corrected fluxes are reported in Tables 7, 8 and 9.

6.3. Galactic and Internal Extinction Correction

The H_{α} fluxes have been then corrected for the galactic extinction due to the gas and the dust of our Galaxy. For each target galaxy we have computed the relative galactic hydrogen column density N_h ($atoms\ cm^{-2}$) as a function of the galaxy coordinates (R.A. and Dec.). N_h was obtained interpolating the data available from the Stark et al. (1992) data-base. We computed also an interpolation error defined as the mean of differences weighted on the distances. Using the relations:

$$\frac{N_h}{A_B - A_V} = \frac{N_h}{E(B - V)} = 5.2 \cdot 10^{21} \ atoms\ cm^{-2}\ mag^{-1} \quad (8)$$

and:

$$R = \frac{A_V}{E(B - V)} = 3.1 \quad (9)$$

(Ryder & Dopita 1994) we have derived the visual extinction coefficients A_V and A_B (*mag*) for each galaxy. Following Ryder & Dopita (1994), we have obtained the multiplicative correction α_G to apply to the H_{α} flux:

$$\alpha_G = 10^{(0.4 \cdot A_{H_{\alpha}})} = 10^{(0.4 \cdot 0.64 A_B)} \quad (10)$$

where $A_{H_{\alpha}}$ is the H_{α} extinction coefficient in magnitudes. The isophotal fluxes corrected for Galactic Extinction are reported in Table 7. The minimum and maximum values obtained for α_G are respectively 1.04 and 2.68.

The H_{α} fluxes of spirals have also been corrected for the Internal Extinction due to the interstellar medium inside the target galaxy itself. This correction in the blue band is usually obtained by summing to the galaxy magnitude the value

$$A_i = c_B \cdot \log(r_i) \quad (11)$$

(Haynes & Giovanelli 1984) where:

c_B is a morphological type dependent correction coefficient in the B band and

r_i is the intrinsic axial ratio of the galaxy.

On the basis of the interstellar extinction curve (e.g. Osterbrook 1974) we have derived the H_{α} extinction correction term $c_{H_{\alpha}}$ using the following transformation:

$$c_B \cdot \log(r_i) - c_{H_{\alpha}} \cdot \log(r_i) = -2.5 \cdot \log(e_B) + 2.5 \cdot \log(e_{H_{\alpha}}) \quad (12)$$

where e_B and $e_{H_{\alpha}}$ are the extinction values at the effective wavelength respectively of the B and the H_{α} filters. Finally we have obtained the flux correction factor $\alpha_i = 10^{[0.4 \cdot c_{H_{\alpha}} \cdot \log(r_i)]}$, to apply to our spiral galaxies. The minimum and maximum values obtained for α_i are respectively 1.1 and 1.6.

On the basis of the fluxes thus obtained we have derived the H_{α} luminosity $L_{H_{\alpha}}$ of galaxies:

$$L_{H_{\alpha}} = 4\pi \cdot f_{H_{\alpha}} \cdot d_L^2 \quad (13)$$

where the luminosity distance d_L is defined as:

$$d_L = \frac{c}{H_0 \cdot q_0^2} \cdot \left(q_0 \cdot z + (q_0 - 1) \cdot [-1 + (2q_0 \cdot z + 1)^{\frac{1}{2}}] \right) \quad (14)$$

We adopted $H_0 = 100\ km\ s^{-1}\ Mpc^{-1}$ and $q_0 = 0.5$.

In Table 7 we report the isophotal luminosities of the galaxies ($L_{iso}(1)$) uncorrected for Galactic and Internal Extinction.

7. Error Estimate

The uncertainties reported in Tables 7, 8 and 9 regarding the different flux estimates have been derived as follows:

$$\sigma_{f_{H_{\alpha}}} = \sqrt{\left(\frac{\partial f_{H_{\alpha}}}{\partial C_{H_{\alpha}}} \cdot \sigma_{C_{H_{\alpha}}} \right)^2 + \left(\frac{\partial f_{H_{\alpha}}}{\partial Z_{flux}} \cdot \sigma_{Z_{flux}} \right)^2 + \left(\frac{\partial f_{H_{\alpha}}}{\partial \alpha_G} \cdot \sigma_{\alpha_G} \right)^2} \quad (15)$$

where:

$C_{H_{\alpha}} = C_{on} - C_{off}$ is the H_{α} instrumental flux;

$\sigma_{C_{H_{\alpha}}}$ is the uncertainty on $C_{H_{\alpha}}$. It is the standard deviation of the stellar flux residuals measured on the net H_{α} images. Since stars do not show H_{α} emission we should not detect any flux at the star positions on the net images. The detection of net counts could be thus represent simple poisson noise and/or no perfect continuum subtraction. Therefore the standard deviation of such measurements gives a good estimation of the pure and not statistical uncertainties on $C_{H_{\alpha}}$;

$\sigma_{Z_{flux}}$ represents the accuracy on the scale factor Z_{flux} (§6.2) and is given by the difference of the zero points derived by the two standard stars observed before and after the target HCG;

σ_{α_G} is the error about the Galactic Extinction α_G (§6.3) derived by the propagation error formula to α_G .

The errors regarding the H_{α} luminosity (Tables 7 and 9) have been calculated by applying the error propagation formula.

8. The H_{α} Catalogue

Table 7 lists the H_{α} isophotal fluxes and luminosities estimated: Col.1: Name of the galaxy (Hickson 1982); Col.2: Flux uncorrected for Galactic and Internal Extinction: f_{iso} (1) ($erg\ cm^{-2}\ s^{-1}$); Col.3: Error about f_{iso} (1): $\sigma_{f_{iso}}(1)$ ($erg\ cm^{-2}\ s^{-1}$); Col.4: Luminosity uncorrected for Galactic and Internal Extinction: L_{iso} (1) ($erg\ s^{-1}$); Col.5: Error about L_{iso} (1): σ_{L_1} (1) ($erg\ s^{-1}$); Col.6: Flux corrected for Galactic Extinction f_{iso} (2) ($erg\ cm^{-2}\ s^{-1}$); Col.7: Error about f_{iso} (2): $\sigma_{f_{iso}}(2)$ ($erg\ cm^{-2}\ s^{-1}$); Col.8: Flux corrected for Galactic and Internal Extinction for spiral galaxies: f_{iso} (3) ($erg\ s^{-1}$); Col.9: Isophotal area at 1σ above the background: A_{iso} ($arcsec^2$); Col.10: S/N ratio computed within the isophotal region defined by the detection threshold.

In Tables 8 and 9 the fluxes are not corrected for Galactic and Internal Extinction. Such corrections can be simply derived from Table 7.

Table 8 lists isophotal corrected and adaptive aperture fluxes:

Col.1: Name of the galaxy (Hickson 1982); Col.2: Isophotal flux f_{isocor} ($erg\ cm^{-2}\ s^{-1}$); Col.3: Error about f_{isocor} : σ_{isocor} ($erg\ cm^{-2}\ s^{-1}$); Col.4: Kron flux f_{Kron} ($erg\ cm^{-2}\ s^{-1}$); Col.5: Error about f_{Kron} : σ_{Kron} ($erg\ cm^{-2}\ s^{-1}$).

In Table 9 we report the fluxes and luminosities of upper limits:

Col.1: Name of the galaxy (Hickson 1982); Col.2: Flux at $3\ \sigma$ above the background ($f_{3\sigma}$) ($erg\ cm^{-2}\ s^{-1}$); Col.3: Error about $f_{3\sigma}$: σ ($erg\ cm^{-2}\ s^{-1}$); Col.4: Luminosity at $3\ \sigma$ above the background ($L_{3\sigma}$) ($erg\ cm^{-2}\ s^{-1}$); Col.5: Error about $L_{3\sigma}$: σ ($erg\ cm^{-2}\ s^{-1}$).

We have compared the estimated f_{iso} , f_{isocor} and f_{Kron} for the detected galaxies by using the Kolmogorov-Smirnov test: we found they are drawn from the same parent population. The distributions of the three different fluxes estimated for the detected galaxies are shown in Figure 3. In the following we make use of f_{iso} in our considerations unless it is differently specified.

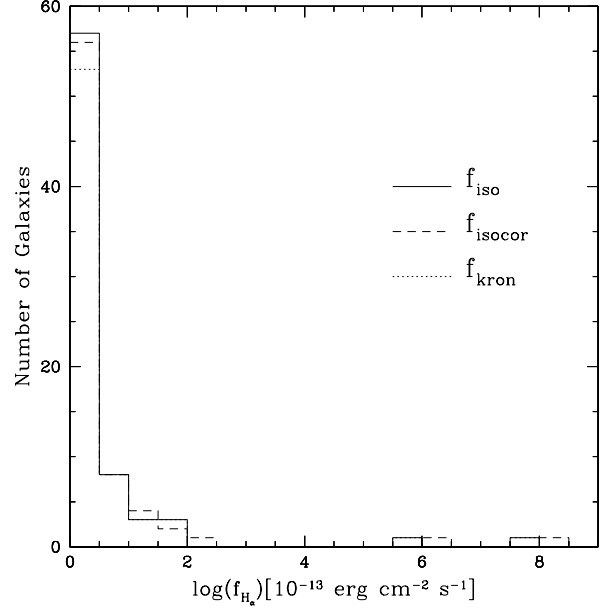


Figure 3: Distribution of f_{iso} (solid line), f_{isocor} (dashed line) and f_{Kron} (dotted line) (corrected for Galactic Extinction) of the 73 detected galaxies. The width of each bin is 0.5 [10^{-13} $erg\ cm^{-2}\ s^{-1}$].

In Figure 4 the distribution of H_{α} isophotal luminosity L_{iso} , corrected for Galactic Extinction and uncorrected for Internal Extinction, of the 73 detected galaxies (shaded histogram) is shown. We over-plot also the distribution of H_{α} upper limits to luminosity for the 22 undetected galaxies (dashed line).

Table 6: Galaxies without estimated flux (see §6.1)

Galaxy	Reason (1,2,3)	Galaxy	Reason (1,2,3)
2c	1	59b	3
15c	1	59c	3
15d	1	59d	3
15f	1	70d	2
34b	2	79a	3
43d	2	79b	3
43e	2	79c	3
47a	2	79d	3
47b	2	81a	3
47c	2	81b	3
47d	2	81c	3
54a	3	81d	3
54b	3	96a	1
54c	3	96b	1
54d	3	96c	1
59a	3	96d	1

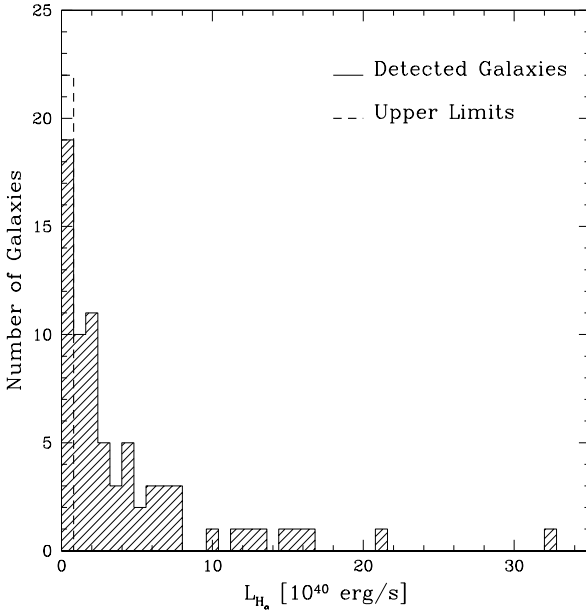


Figure 4: Distribution of H_{α} luminosity, corrected for Galactic Extinction, for both the 73 detected galaxies (shaded histogram) and for the 22 upper limits (dashed line). The width of each bin is 0.8 [10^{40} erg s $^{-1}$].

9. Star formation Rate

So far this is the largest H_{α} catalogue of HCG galaxies having H_{α} calibrated fluxes. Such a sample constitutes a powerful tool to perform quantitative analysis on the recent star formation rate inside HCG galaxies. We have derived the *SFR* for the galaxies of our sample using the results of Kennicutt (1983), which relate the *SFR* to H_{α} luminosity through the relation:

$$SFR(\text{total}) = \frac{L(H_{\alpha})}{1.12 \cdot 10^{41} \text{erg s}^{-1}} M_{\odot} \text{yr}^{-1} \quad (16)$$

where a Salpeter initial mass function with an upper mass cutoff of $100 M_{\odot}$ has been assumed. *SFR* inferred from luminosities for the 73 galaxies detected and for 22 upper limits estimated is shown in Table 10 as follows:

- Col. 1: Name of detected galaxies;
- Col. 2: *SFR* inferred from isophotal luminosities L_{iso} corrected for Galactic Extinction, SFR_{iso} (2) ;
- Col. 3: *SFR* inferred from isophotal luminosities, corrected for both Galactic and Internal Extinction, SFR_{iso} (3);
- Col. 5: Name of galaxies for which we have computed the upper limits;
- Col. 6: *SFR* inferred from upper limit to luminosity, corrected for Galactic Extinction, SFR_{ul} (2);
- Col. 7: *SFR* inferred from upper limit to luminosity, corrected for both Galactic and Internal Extinction, SFR_{ul} (3);

In Figure 5 we show the distribution of SFR_{iso} computed taking into account (dotted line) and without taking into

account (solid line) Internal Extinction. The two distributions are quite similar, as confirmed also by a Kolmogorov-Smirnov test.

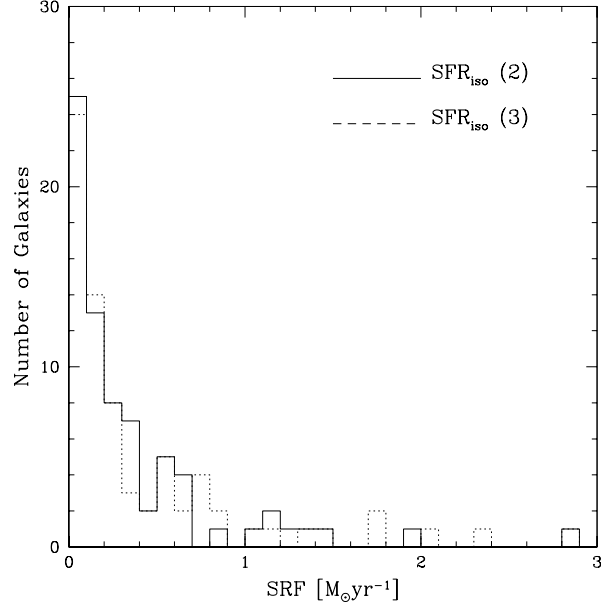


Figure 5: Distribution of *SFR* for the 73 detected galaxies derived from L_{iso} . The solid histogram represents the SFR_{iso} (2) and the dotted histogram represents the SFR_{iso} (3) (see Table 10). The width of each bin is 0.1 [M_{\odot} yr $^{-1}$].

10. Discussion

Figures 6 to 11 show the continuum and H_{α} maps of some of the HCG galaxies of our sample. A isocontour plot is also shown for the largest galaxies of these groups. In the H_{α} images we have removed residuals of field stars for clarity and we display the galaxy flux one sigma above the background. The scale of the axes are in pixel units and the field of view is 5.12x5.12 arcmin. East is on the top and North on the left. For each image the name of HCG is shown in the caption, while the name of the galaxies are reported in the figure. In the following we present a brief description of the groups and galaxies in figures 6 to 11. The values regarding the flux of the lowest isocontours are corrected for Galactic Extinction.

HCG2- This group consists of a triplet of galaxies with accordant redshifts (galaxies a, and c) plus a fainter member (galaxy d) which has a higher redshift. In Figure 6 are included only the galaxies a and b, for which we have estimated the H_{α} fluxes. Galaxy a (late type barred spiral) is brighter in H_{α} than b (compact irregular), which is also a infrared source. In the H_{α} map some knots are resolved in the disk of galaxy a. For galaxy b we detect

a strong H_{α} emission in the center and no emission in the outer part, as previously noted by Vilchez & Iglesias Paramo 1998a. The estimated SFR_{iso} for a and b are respectively 1.45 and $1.16 M_{\odot} \text{ yr}^{-1}$. In the lowest panel of Figure 6 the isocontour plot, showing the shape and the orientation of the H_{α} emission, is given. The lowest contour is at 1σ above the background, corresponding to an H_{α} emission of $6.27 \cdot 10^{-17} \text{ erg cm}^2 \text{s}^{-1} \text{arcsec}^{-2}$. The interval among the contours is 3σ . The H_{α} emitting areas have an extension of about 1643.6 and 315.8 arcsec^2 for a and b galaxies respectively.

HCG37- This is a compact group with five accordant galaxies: a and b are the dominant galaxies of the group. They are radio sources, as galaxy d. The group has a high velocity dispersion (398.1 km s^{-1}) and mass-to-light ratio ($123 M_{\odot} L_{\odot}$), and a short crossing time ($0.0054 Ht_c$). The H_{α} brightest source of the group is galaxy a. This is a blue elliptical galaxy with a rapidly rotating central disk of ionized gas (Rubin et al. 1991). Galaxy b is an edge-on spiral with an intensive H_{α} emission in the center. This galaxy is also an infrared source. Galaxies c (SOa), d (SBdm) and e (E0) are all fainter H_{α} emitters than galaxies a and b. The SFR_{iso} estimated for a, b, c, d and e galaxies are respectively 0.26, 0.13, 0.03, 0.08 and $0.02 M_{\odot} \text{ yr}^{-1}$. The lowest panel of Figure 7 presents the isocontours for the largest galaxies of the group: the extensions of H_{α} emission are of about 235.2, 217.1, 46.7, 98.4 and 28.4 arcsec^2 for a, b, c, d and e galaxies respectively. The lowest contour is at 1σ above the background, that is H_{α} emission higher than $3.64 \cdot 10^{-17} \text{ erg cm}^2 \text{s}^{-1} \text{arcsec}^{-2}$, while the interval among the contours is 3σ .

HCG38- This group contains the interacting pair Arp 237 (galaxies b and c) with one other galaxy at a similar redshift (galaxy a), plus a fainter high-redshift galaxy (d). Galaxy a is a spiral showing an H_{α} emission more intense in the center than in the outer disk. The H_{α} brightest galaxy b (late type barred spiral) is in the interacting pair and it is an infrared source. In galaxy b we reveal a strong H_{α} emission in the central part of the galaxy and some resolved knots throughout its arm placed in the direction opposite to galaxy c. This last galaxy is of irregular type and it is the H_{α} dimmest galaxy of the group. The estimated SFR_{iso} for a, b and c are respectively 0.34, 0.39 and $0.19 M_{\odot} \text{ yr}^{-1}$. The isocontour plots in Figure 8 show the H_{α} emission higher than $7.22 \cdot 10^{-17} \text{ erg cm}^2 \text{s}^{-1} \text{arcsec}^{-2}$ (1σ above the background). The interval among the contours is 1σ . The extensions of H_{α} emission are of about 156.3, 150.4 and 60.0 arcsec^2 for a, b and c galaxies respectively.

HCG46- This group consists of four early-type galaxies. The velocity dispersion and mass-to-light ratio of the group is relatively high (respectively 323.6 km s^{-1} and

$478.6 M_{\odot}/L_{\odot}$). Galaxies b and c appear to be in contact in the continuum image, but not in the H_{α} map. Two features are in common to all the galaxies of the group: they show a faint H_{α} emissions that seems confined to the bulge of galaxies. The estimated SFR_{iso} for a, b, c and d are respectively 0.04, 0.03, 0.01 and $0.002 M_{\odot} \text{ yr}^{-1}$. The extensions of H_{α} emission at 1σ above the background are reported in Table 7.

HCG49- This is a small and very compact group with four accordant galaxies. Its median galaxy separation is only of $12.3 h^{-1} \text{kpc}$ and its velocity dispersion is so low (lower than the uncertainties in the velocity measurements) that no estimate can be made of its mass-to-light ratio (Hickson 1993). Galaxies a and b are spiral, while c is an irregular and d an elliptical. Galaxy b is the H_{α} brightest source of the group, while galaxies a, c and d have comparable H_{α} emission among them. The estimated SFR_{iso} for a, b, c and d are respectively 0.56, 1.3, 0.26 and $0.14 M_{\odot} \text{ yr}^{-1}$. In the lowest panel of Figure 10 the isocontour plot is shown. The lowest contour is at 1σ above the background, corresponding to an H_{α} emission of $9.44 \cdot 10^{-17} \text{ erg cm}^2 \text{s}^{-1} \text{arcsec}^{-2}$. The interval among the contours is 2σ . The extensions of H_{α} emission are of about 72.8, 96.3, 48.9 and 27 arcsec^2 for a, b, c and d galaxies respectively.

HCG74- This group contains five early-type accordant galaxies: a, b, d are elliptical and c and e are lenticular. Galaxy a is the dominant one with two very close companions (b and c) and it is also a radio source. All galaxies show an H_{α} emission confined to their center. We have not revealed e galaxy for which we have estimated the upper limit. The estimated SFR_{iso} for a, b, c and d detected galaxies are respectively 0.51, 0.12, 0.1 and $0.1 M_{\odot} \text{ yr}^{-1}$. In the lowest panel of Figure 11 the isocontour plots for a, b and c galaxies are shown. The lowest contour is at 1σ above the background ($7.52 \cdot 10^{-17} \text{ erg cm}^2 \text{s}^{-1} \text{arcsec}^{-2}$), while the interval among the contours is 1σ . The extensions of H_{α} emission are 61.38, 40.59, 21.96 and 23.04 arcsec^2 for a, b, c and d galaxies respectively.

11. Summary

We have obtained H_{α} fluxes and luminosities for a sample of 95 galaxies from calibrated observations of 31 HCGs. The sample thus collected comprises 75% of the accordant galaxies of the observed groups and it represents the largest H_{α} selected sample of HCG galaxies so far having calibrated fluxes. By the estimated $L_{H_{\alpha}}$ we have obtained the star formation rate of the sample galaxies. In a following paper (Sevrgnini & Saracco, 1999) we will combine the results obtained from the data presented here with dynamical, morphological and broad band photomet-

rical data from the literature (Hickson 1982, Hickson 1993, Rood & Struble 1994) to show that the H_{α} luminosity of galaxies and hence their current star formation rate are affected by the dynamics of groups in which they reside. Further analysis based on these H_{α} data will allow us to study the rate of interaction and merger phenomena occurring in HCGs, yielding new insights about the formation and evolution of these systems.

Acknowledgements. We are grateful to E. Recillas and D. Maccagni which have kindly carried out one of the observing runs. We would like also to thank the S. Pedro Martir observatory staff for the helpful support given during observations. PS would like to acknowledge and to thank B. Catinella and S. Molendi for the useful discussions and suggestions given during this work was in progress.

References

Bertin E. & Arnouts S. 1996, A&A 313L, 21
 Fukugita M., Shimasaku K. & Ichikawa T. 1995, PASP 107, 945
 Haynes M.P.e Giovanelli R. 1984, AJ 89, 758
 Hickson P. 1982, ApJ 255, 382
 Hickson P. 1993, ApJL V.29:1-3, P.1 *Atlas of Compact Groups of Galaxies*
 Hickson P., Kindl E., Auman J.R. 1989a, ApJS 70, 687
 Hickson P., Mendes de Oliveira C., Hucra J.P. & Palumbo G.G.C. 1992, ApJ 399, 353
 Iglesias Paramo J. & Vilchez J.M. 1999, astroph/9902336
 Kennicutt R.C. 1983, ApJ 272, 54
 Kennicutt R.C. & Kent S. 1983, AJ 88, 1094
 Kron R.G. 1980, ApJS 43, 305
 Massey P., Strobel K., Barnes J.V. & Anderson E. 1988, ApJ 328, 315
 Mendes de Oliveira C.M., Amaram P., Balkowski C. & Boulesteix J. 1997, ASP Conf. Ser., Vol. 117, 156
 Mendes de Oliveira C.M. & Hickson P. 1994, ApJ 427, 684
 Mendes de Oliveira C.M., Plana H., Amaram P., Bolte M. & Boulesteix J. 1998, ApJ 507, 691
 Moles M., del Olmo A., Perea J., Masegosa J., Marquez I. & Costa V. 1994, A&A 285, 404
 Osterbrock D.E. 1974, in *Astrophysics of Gaseous Nebulae*, W.H. Free man and Company
 Plana H., Mendes de Oliveira C.M., Amaram P. & Boulesteix J. 1998, AJ 116, 2123
 Pogge R.W. 1992, ASP Conference Series, Vol. 23, 198P.
 Rood H.J. & Struble M.F. 1994, P.A.S.P. 106, 413
 Rubin V.C., Hunter D.A. & Ford W.K. 1991, ApJS 76, 153
 Ryder S.D. & Dopita M.A. 1994, ApJ 430, 142
 Severgnini P. & Saracco P. 1999, Ap. & Sp. Science, submitted
 Stark A.A. et al. 1992, ApJS 79, 77
 Valluri M. & Anupama G.C. 1996, AJ 112, 1390V
 Vorontsov-Vel'yaninov B.A. 1959, *Atlas and Catalogue of interacting Galaxies*, Vol.1 (Sternberg Institute, Moscow State University, Moscow)
 Vilchez J.M. & Iglesias Paramo J. 1998a, ApJS 117, 1
 Vilchez J.M. & Iglesias Paramo J. 1998b, ApJ 506, L101
 Zepf S.E. 1993, ApJ 407, 448
 Zepf S.E., Whitmore B.C. & Levison H.F. 1991, ApJ 383, 524
 Zombeck M.V. 1990, *Handbook of Space Astronomy and Astrophysics*, Cambridge University Press

Table 2: Principal features of the observed galaxies (Hickson 1993): Galaxy name, heliocentric velocity of group, total photographic blue magnitude, morphological type of galaxy.

Galaxy	V ($Km\ s^{-1}$)	B_T	T	Galaxy	V ($Km\ s^{-1}$)	B_T	T	Galaxy	V ($Km\ s^{-1}$)	B_T	T
2a	4326	13.35	SBd	56a	8245	15.24	Sc	82a	11177	14.14	E3
2b	4366	14.39	cI	56b	7919	14.5	SB0	82b	10447	14.62	SBa
2c	4235	14.15	SBc	56c	8110	15.37	S0	82c	10095	14.78	Im
15c	7222	14.37	E0	56d	8346	16.52	S0	82d	11685	15.95	S0a
15d	6244	14.65	E2	56e	7924	16.23	S0	83a	15560	15.99	E0
15f	6242	15.74	Sbc	59a	4109	14.52	Sa	83b	16442	16.04	E2
33a	7570	15.35	E1	59b	3908	15.2	E0	83c	16520	16.7	Sed
33b	8006	15.41	E4	59c	4347	14.4	Sc	83d	15500	17.91	Sd
33c	7823	16.4	Sd	59d	3866	15.8	Im	83e	15560	18.4	S0
33d	7767	16.73	E0	66a	20688	15.38	E1	92b	5774	13.18	Sbc
34a	8997	14.2	E2	66b	21472	16.5	S0	92c	6764	13.33	SBa
34b	9620	16.56	Sd	66c	20801	16.39	S0	92d	6630	13.63	SB0
34c	9392	16.28	SBd	66d	20850	17.45	E2	92e	6599	14.01	Sa
34d	8817	17.57	S0	68a	2162	11.84	S0	96a	8698	13.53	Sc
35a	15919	15.56	S0	68b	2635	12.24	E2	96b	8616	14.49	E2
35b	16338	15.13	E1	69a	8856	14.94	Sc	96c	8753	15.69	Sa
35c	16357	15.69	E1	69b	8707	15.59	SBb	96d	8975	16.56	Im
35d	15798	16.81	Sb	69c	8546	14.94	S0				
35e	16773	17.05	S0	69d	9149	16.06	SB0				
35f	16330	18.12	E1	70d	18846	15.42	Sc				
37a	6745	12.97	E7	70e	19117	15.91	Sbc				
37b	6741	14.5	Sbc	70f	19243	16.4	SBb				
37c	7357	15.57	S0a	70g	19010	16.39	Sa				
37d	6207	15.87	Sbdm	71a	9320	13.75	SBc				
37e	6363	16.21	E0	71b	9335	14.9	Sb				
38a	8760	15.25	Sbc	71c	8450	15.56	SBc				
38b	8739	14.76	SBd	72a	12506	13.86	Sa				
38c	8770	15.39	Im	72b	12356	15.48	S0				
43a	10163	15.13	Sb	72c	13062	15.47	E2				
43b	10087	15.18	SBcd	72d	12558	15.64	SB0				
43c	9916	15.82	SB0	74a	12255	14.06	E1				
43d	9630	16.82	Sc	74b	12110	15.07	E3				
43e	9636	17.2	S0	74c	12266	16.1	S0				
45a	21811	15.2	Sa	74d	11681	16.32	E2				
45b	22195	17.24	S0a	74e	11489	17.8	S0				
45c	21799	17.6	Sc	75a	12538	15.2	E4				
46a	8201	16.4	E3	75b	12228	14.9	Sb				
46b	8571	16.28	S0	75c	12292	15.93	S0				
46c	7906	16.13	E1	75d	12334	15.82	Sd				
46d	7703	16.11	SB0	75e	12300	16.36	Sa				
47a	9581	14.61	SBb	75f	13080	16.66	S0				
47b	9487	15.67	E3	76a	10054	15.08	Sa				
47c	9529	16.63	Sc	76b	10002	14.44	E2				
47d	9471	16.2	Sd	76c	10663	14.73	E0				
49a	9939	15.87	Scd	76d	10150	15.21	E1				
49b	9930	16.3	Sd	76e	10328	16.65	SB0				
49c	9926	17.18	Im	76f	10216	16.48	Sc				
49d	10010	16.99	E5	79a	4294	14.35	E0				
53a	6261	12.91	SBbc	79b	4446	13.78	S0				
53b	6166	14.73	S0	79c	4146	14.72	S0				
53c	6060	14.81	SBs	79d	4503	15.87	Sdm				
54a	1397	13.86	Sdm	81a	14676	16.25	Sc				
54b	1412	16.08	Im	81b	15150	16.51	S0				
54c	1420	16.8	Im	81c	15050	17.18	S0				
54d	1670	18.02	Im	81d	14954	17.14	S0a				

Table 7: Isophotal Fluxes and Luminosities

Galaxy	f_{iso} (1)	$\sigma_{f_{iso}}$ (1)	L_{iso} (1)	$\sigma_{L_{iso}}$ (1)	f_{iso} (2)	$\sigma_{f_{iso}}$ (2)	f_{iso} (3)	A_{iso}	S/N
	($\frac{erg}{cm^2 s}$)	($\frac{erg}{cm^2 s}$)	($\frac{erg}{s}$)	($\frac{erg}{s}$)	($\frac{erg}{cm^2 s}$)	($\frac{erg}{cm^2 s}$)	($\frac{erg}{cm^2 s}$)	($arcsec^2$)	
2a	6.29E-13	3E-14	1.39E+41	6E+39	7.60E-13	3E-14	9.12E-13	1643.6	890
2b	4.94E-13	2E-14	1.07E+41	5E+39	5.98E-13	3E-14		315.8	1584
33a	5.69E-15	9E-16	3.73E+39	6E+38	1.52E-14	2E-15		20.3	99
33b	3.16E-15	9E-16	2.32E+39	6E+38	8.47E-15	2E-15		16.1	60
33c	4.03E-14	3E-15	2.82E+40	2E+39	1.08E-13	7E-15	1.12E-13	269.6	191
33d	1.18E-15	8E-16	8.16E+38	6E+38	3.17E-15	2E-15		8.2	32
34c	3.76E-14	1E-14	3.81E+40	1E+40	7.57E-14	3E-14	9.33E-14	74.9	68
35a	1.46E-14	2E-15	4.29E+40	6E+39	1.66E-14	2E-15		25.6	108
35b	8.15E-15	2E-15	2.53E+40	6E+39	9.28E-15	2E-15		21.9	67
35c	9.16E-15	2E-15	2.85E+40	6E+39	1.04E-14	2E-15		25.7	69
35d	8.95E-15	2E-15	2.59E+40	5E+39	1.02E-14	2E-15	1.10E-14	35.7	59
35e	2.09E-15	2E-15	6.84E+39	6E+39	2.38E-15	2E-15		19.4	18
35f	1.19E-15	2E-15	3.69E+39	6E+39	1.36E-15	2E-15		5.1	20
37a	5.12E-14	9E-15	2.66E+40	5E+39	5.65E-14	1E-14		235.2	328
37b	2.49E-14	9E-15	1.29E+40	5E+39	2.74E-14	1E-14	3.77E-14	217.1	166
37c	5.17E-15	9E-15	3.20E+39	6E+39	5.71E-15	1E-14		46.7	75
37d	1.74E-14	1E-14	7.68E+39	5E+39	1.93E-14	1E-14		98.4	129
37e	3.35E-15	1E-14	1.55E+39	5E+39	3.69E-15	1E-14		28.4	51
38a	3.67E-14	5E-15	3.23E+40	4E+39	4.31E-14	6E-15	4.60E-14	156.3	147
38b	4.29E-14	5E-15	3.76E+40	5E+39	5.03E-14	6E-15	6.53E-14	150.4	175
38c	2.06E-14	4E-15	1.82E+40	3E+39	2.41E-14	4E-15		60.0	133
43a	5.34E-14	4E-15	6.34E+40	4E+39	6.19E-14	4E-15	6.32E-14	210.6	190
43b	4.79E-14	3E-15	5.6E+40	4E+39	5.55E-14	4E-15	7.01E-14	174.4	177
43c	2.36E-14	2E-15	2.67E+40	2E+39	2.74E-14	2E-15		105.3	82
45a	3.70E-14	2E-15	2.06E+41	1E+40	3.85E-14	2E-15	4.81E-14	150.4	136
45b	7.10E-15	2E-15	4.1E+40	1E+40	7.39E-15	2E-15		26.7	60
45c	2.78E-15	2E-15	1.55E+40	1E+40	2.89E-15	2E-15	3.52E-15	14.0	32
46a	4.72E-15	7E-16	3.63E+39	5E+38	5.42E-15	8E-16		29.7	71
46b	3.08E-15	6E-16	2.60E+39	5E+38	3.54E-15	7E-16		17.4	60
46c	1.45E-15	6E-16	1.04E+39	4E+38	1.66E-15	7E-16		15.1	31
46d	2.96E-16	6E-16	2.01E+38	4E+38	3.41E-16	7E-16		8.0	8.9
49a	5.05E-14	2E-15	5.74E+40	2E+39	5.47E-14	2E-15	8.64E-14	72.8	162
49b	1.18E-13	4E-15	1.34E+41	5E+39	1.28E-13	5E-15	1.75E-13	96.3	330
49c	2.35E-14	2E-15	2.67E+40	2E+39	2.55E-14	2E-15		48.9	92
49d	1.21E-14	1E-15	1.40E+40	1E+39	1.31E-14	1E-15		27.0	72
53a	1.44E-13	4E-15	6.44E+40	2E+39	1.55E-13	4E-15	1.55E-13	429.4	162
53b	1.48E-14	4E-15	6.41E+39	2E+39	1.59E-14	4E-15		38.4	56
53c	9.37E-14	4E-15	3.93E+40	2E+39	1.01E-13	4E-15	1.30E-13	155.3	177

Table 7: Continued

Galaxy	f_{iso} (1)	$\sigma_{f_{iso}}$ (1)	L_{iso} (1)	$\sigma_{L_{iso}}$ (1)	f_{iso} (2)	$\sigma_{f_{iso}}$ (2)	f_{iso} (3)	A_{iso}	S/N
	($\frac{erg}{cm^2 s}$)	($\frac{erg}{cm^2 s}$)	($\frac{erg}{s}$)	($\frac{erg}{s}$)	($\frac{erg}{cm^2 s}$)	($\frac{erg}{cm^2 s}$)	($\frac{erg}{cm^2 s}$)	($arcsec^2$)	
56a	2.15E-14	1E-15	1.68E+40	8E+38	2.26E-14	1E-15	2.65E-14	131.7	87
56b	1.58E-13	3E-15	1.13E+41	2E+39	1.66E-13	3E-15		150.6	601
56d	2.78E-14	1E-15	2.22E+40	9E+38	2.93E-14	1E-15		68.5	156
56e	7.86E-15	9E-16	5.65E+39	7E+38	8.26E-15	1E-15		39.5	58
66b	5.64E-14	4E-15	3.04E+41	2E+40	5.99E-14	4E-15		30.7	579
69a	8.13E-15	2E-15	7.32E+39	1E+39	8.67E-15	2E-15	1.05E-14	56.6	45
69b	4.43E-14	4E-15	3.86E+40	4E+39	4.73E-14	4E-15	6.75E-14	50.4	193
70e	2.22E-14	9E-16	9.46E+40	4E+39	2.35E-14	1E-15	3.71E-14	43.7	60
70g	1.14E-14	7E-16	4.87E+40	3E+39	1.21E-14	7E-16	1.92E-14	39.8	42
71a	1.45E-13	7E-15	1.45E+41	7E+39	1.56E-13	7E-15	2.31E-13	571.7	342
71b	8.71E-15	8E-16	8.72E+39	8E+38	9.36E-15	8E-16	1.04E-14	97.7	50
71c	2.62E-14	1E-15	2.14E+40	1E+39	2.81E-14	1E-15	3.94E-14	228.8	162
72a	8.12E-15	2E-15	1.47E+40	4E+39	9.04E-15	2E-15	1.19E-14	34.7	43
72b	3.81E-15	2E-15	6.72E+39	4E+39	4.24E-15	2E-15		18.0	28
72c	2.98E-15	2E-15	5.87E+39	4E+39	3.32E-15	2E-15		10.9	28
72d	3.83E-15	2E-15	6.97E+39	4E+39	4.26E-15	2E-15		13.2	33
74a	2.73E-14	2E-15	4.73E+40	3E+39	3.27E-14	2E-15		61.4	169
74b	6.56E-15	7E-16	1.11E+40	1E+39	7.84E-15	9E-16		40.6	52
74c	5.18E-15	7E-16	8.98E+39	1E+39	6.19E-15	9E-16		22.0	53
74d	5.73E-15	7E-16	9.01E+39	1E+39	6.85E-15	8E-16		23.0	63
75a	2.96E-14	1E-15	5.37E+40	2E+39	3.56E-14	1E-15		137.6	86
75b	6.22E-15	6E-16	1.07E+40	1E+39	7.48E-15	7E-16	8.64E-15	21.1	46
75c	9.06E-15	7E-16	1.58E+40	1E+39	1.09E-14	8E-16		54.6	42
75d	2.95E-14	1E-15	5.19E+40	2E+39	3.56E-14	1E-15	4.50E-14	96.3	148
75f	1.36E-15	4E-16	2.69E+39	8E+38	1.64E-15	5E-16		44.1	10
76a	1.20E-14	2E-15	1.39E+40	2E+39	1.42E-14	2E-15	1.69E-14	23.3	61
76b	1.17E-14	2E-15	1.35E+40	2E+39	1.4E-14	2E-15		55.8	38
76c	1.1E-14	2E-15	1.44E+40	2E+39	1.31E-14	2E-15		57.4	33
76d	1.18E-14	2E-15	1.4E+40	2E+39	1.40E-14	2E-15		54.6	33
76f	5.60E-15	2E-15	6.72E+39	2E+39	6.91E-15	2E-15	9.37E-15	13.1	36
82b	4.17E-15	1E-15	5.23E+39	2E+39	4.51E-15	2E-15	4.49E-15	32.5	23
82c	3.38E-14	2E-15	3.96E+40	2E+39	3.66E-14	2E-15		83.4	109
83b	1.31E-15	1E-15	4.12E+39	3E+39	1.71E-15	1E-15		21.4	8
83c	3.03E-14	3E-15	9.59E+40	9E+39	3.95E-14	4E-15	4.95E-14	69.3	104
92c	5.10E-14	3E-15	2.67E+40	1E+39	7.25E-14	4E-15	1.07E-13	120.9	164

Table 8: Isophotal Corrected and Kron Fluxes

Galaxy	f_{isocor}	σ_{isocor}	f_{Kron}	σ_{Kron}	Galaxy	f_{isocor}	σ_{isocor}	f_{Kron}	σ_{Kron}
	$(\frac{erg}{cm^2 s})$	$(\frac{erg}{cm^2 s})$	$(\frac{erg}{cm^2 s})$	$(\frac{erg}{cm^2 s})$		$(\frac{erg}{cm^2 s})$	$(\frac{erg}{cm^2 s})$	$(\frac{erg}{cm^2 s})$	$(\frac{erg}{cm^2 s})$
2a	6.64E-13	3E-14	6.37E-13	3E-14	74a	2.87E-14	2E-15	2.45E-14	2E-15
2b	4.99E-13	2E-14	4.93E-13	2E-14	74b	6.89E-15	8E-16	6.78E-15	8E-16
33a	6.05E-15	9E-16	5.38E-15	9E-16	74c	6.27E-15	8E-16	3.99E-15	7E-16
33b	3.56E-15	9E-16	2.60E-15	8E-16	74d	6.6E-15	7E-16	4.65E-15	7E-16
33c	4.65E-14	3E-15	4.46E-14	3E-15	75a	3.75E-14	1E-15	1.86E-14	9E-16
33d	1.45E-15	8E-16	6.50E-16	8E-16	75b	7.87E-15	6E-16	6.96E-15	6E-16
34c	5.54E-14	1E-14	4.47E-14	1E-14	75c	1.24E-14	7E-16	8.22E-15	6E-16
35a	1.57E-14	2E-15	1.34E-14	2E-15	75d	3.27E-14	1E-15	3.12E-14	1E-15
35b	8.31E-15	2E-15	8.75E-15	2E-15	75f	2.42E-15	4E-16		
35c	9.20E-15	2E-15	9.01E-15	2E-15	76a	1.28E-14	2E-15	1.25E-14	2E-15
35d	1.03E-14	2E-15	9.70E-15	2E-15	76b	1.09E-14	2E-15		
35e	1.93E-15	2E-15	2.58E-15	2E-15	76c	1.01E-14	2E-15		
35f	1.73E-15	2E-15	1.20E-15	2E-15	76d	1.14E-14	2E-15		
37a	5.45E-14	9E-15	5.07E-14	9E-15	76f	7.08E-15	2E-15	5.02E-15	2E-15
37b	3.01E-14	9E-15	2.74E-14	9E-15	82b	5.52E-15	1E-15	8.79E-16	1E-15
37c	6.25E-15	9E-15	5.36E-15	9E-15	82c	3.98E-14	2E-15	3.47E-14	2E-15
37d	1.98E-14	1E-14	1.84E-14	1E-14	83b	1.46E-15	1E-15	2.32E-15	1E-15
37e	4.31E-15	1E-14	3.64E-15	1E-14	83c	3.46E-14	3E-15	3.26E-14	3E-15
38a	4.34E-14	5E-15	3.89E-14	5E-15	92c	5.66E-14	3E-15	5.28E-14	3E-15
38b	4.87E-14	6E-15	4.55E-14	6E-15					
38c	2.24E-14	4E-15	2.13E-14	4E-15					
43a	6.15E-14	4E-15	5.34E-14	4E-15					
43b	5.42E-14	4E-15	4.93E-14	3E-15					
43c	3.07E-14	2E-15	2.63E-14	2E-15					
45a	4.64E-14	2E-15	4.95E-14	2E-15					
45b	8.54E-15	2E-15	7.59E-15	2E-15					
45c	3.9E-15	2E-15	5.03E-15	2E-15					
46a	5.48E-15	7E-16	4.76E-15	7E-16					
46b	3.47E-15	7E-16	2.95E-15	6E-16					
46c	1.63E-15	6E-16	1.36E-15	6E-16					
46d	3.55E-16	6E-16	7.21E-17	6E-16					
49a	5.47E-14	2E-15	5.21E-14	2E-15					
49b	1.22E-13	4E-15	1.20E-13	4E-15					
49c	2.66E-14	2E-15	2.47E-14	2E-15					
49d	1.25E-14	1E-15	1.28E-14	1E-15					
53a	2.1E-13	4E-15	1.84E-13	4E-15					
53b	1.69E-14	4E-15	1.57E-14	4E-15					
53c	1.05E-13	4E-15	9.76E-14	4E-15					
56a	3.15E-14	1E-15	2.65E-14	1E-15					
56b	1.59E-13	3E-15	1.58E-13	3E-15					
56d	2.98E-14	1E-15	2.81E-14	1E-15					
56e	8.46E-15	9E-16	8.64E-15	9E-16					
66b	5.87E-14	4E-15	7.98E-15	5E-16					
69a	1.06E-14	2E-15	1.18E-14	2E-15					
69b	4.62E-14	4E-15	4.46E-14	4E-15					
70e	2.90E-14	1E-15	2.43E-14	1E-15					
70g	1.3E-14	7E-16	1.03E-15	6E-16					
71a	1.64E-13	8E-15	1.49E-13	7E-15					
71b	6.96E-15	7E-16	1.12E-14	8E-16					
71c	3.22E-14	2E-15	2.96E-14	1E-15					
72a	8.44E-15	2E-15	8.40E-15	2E-15					
72b	3.95E-15	2E-15	3.94E-15	2E-15					
72c	2.92E-15	2E-15	2.93E-15	2E-15					
72d	4.14E-15	2E-15	4.27E-15	2E-15					

Table 9: Upper Limit to Flux and Luminosity

Galaxy	$f_{3\sigma}$ ($erg\ cm^{-2}s^{-1}$)	σ ($erg\ cm^{-2}s^{-1}$)	$L_{3\sigma}$ ($erg\ s^{-1}$)	σ ($erg\ s^{-1}$)
34a	8.08E-17	1E-14	7.51E+37	9E+39
34d	7.19E-17	8E-15	6.41E+37	8E+39
56c	1.29E-16	9E-16	9.76E+37	7E+38
66a	7.82E-17	5E-18	3.91E+38	2E+37
66c	7.82E-17	5E-18	3.96E+38	2E+37
66d	7.82E-17	5E-18	3.98E+38	2E+37
68a	1.45E-16	2E-15	7.69E+36	8E+37
68b	1.50E-16	2E-15	1.18E+37	1E+38
69c	1.86E-16	2E-15	1.55E+38	2E+39
69d	2.50E-16	3E-15	2.40E+38	3E+39
70f	2.56E-16	6E-16	1.10E+39	3E+39
74e	1.19E-16	6E-16	1.81E+38	8E+38
75e	1.30E-16	4E-16	2.27E+38	7E+38
76e	2.39E-16	2E-15	2.94E+38	2E+39
82a	1.72E-16	1E-15	2.47E+38	2E+39
82d	1.74E-16	1E-15	2.74E+38	2E+39
83a	2.20E-16	2E-15	6.18E+38	3E+39
83d	2.06E-16	1E-15	5.73E+38	3E+39
83e	2.07E-16	1E-15	5.81E+38	3E+39
92b	2.32E-16	3E-15	8.84E+37	1E+39
92d	1.73E-16	2E-15	8.69E+37	1E+39
92e	1.73E-16	2E-15	8.62E+37	1E+39

Table 10: SFR of galaxies in the sample

Galaxy	SFR_{iso} (2)	SFR_{iso} (3)	Galaxy	SFR_{iso} (2)	SFR_{iso} (3)	Upper Limits	SFR_{ul} (2)	SFR_{ul} (3)
	$M_{\odot} \text{ yr}^{-1}$	$M_{\odot} \text{ yr}^{-1}$		$M_{\odot} \text{ yr}^{-1}$	$M_{\odot} \text{ yr}^{-1}$		$M_{\odot} \text{ yr}^{-1}$	$M_{\odot} \text{ yr}^{-1}$
2a	1.4465	1.7363	53c	0.3780	0.4860	34a	0.0014	0.0014
2b	1.1584	1.1584	56a	0.1572	0.1842	34d	0.0012	0.0011
33a	0.0892	0.0892	56b	1.0621	1.0621	56c	0.0009	0.0009
33b	0.0556	0.0556	56d	0.2085	0.2085	66a	0.0037	0.0037
33c	0.6754	0.7032	56e	0.0530	0.0530	66c	0.0038	0.0038
33d	0.0196	0.0196	66b	2.8838	2.8838	66d	0.0038	0.0038
34c	0.6843	0.8435	69a	0.0697	0.0844	68a	7E-05	7E-05
35a	0.4360	0.4360	69b	0.3669	0.5241	68b	0.0001	0.0001
35b	0.2569	0.2569	70e	0.8952	1.4116	69c	0.0015	0.0015
35c	0.2893	0.2893	70g	0.4604	0.7295	69d	0.0023	0.0023
35d	0.2633	0.2845	71a	1.3874	2.0588	70f	0.0105	0.0154
35e	0.0695	0.0695	71b	0.0836	0.0926	74e	0.0019	0.0019
35f	0.0375	0.0375	71c	0.2055	0.2877	75e	0.0024	0.0033
37a	0.2623	0.2623	72a	0.1457	0.1909	76e	0.0031	0.0031
37b	0.1273	0.1748	72b	0.0668	0.0668	82a	0.0024	0.0024
37c	0.0316	0.0316	72c	0.0584	0.0584	82d	0.0027	0.0027
37d	0.0757	0.0757	72d	0.0693	0.0693	83a	0.0072	0.0072
37e	0.0153	0.0153	74a	0.5054	0.5054	83d	0.0067	0.01
38a	0.3385	0.3614	74b	0.1185	0.11845	83e	0.0068	0.0068
38b	0.3933	0.5111	74c	0.0959	0.0959	92b	0.0011	0.0013
38c	0.1901	0.1901	74d	0.0962	0.0962	92d	0.0011	0.0011
43a	0.6562	0.6701	75a	0.5775	0.5775	92e	0.0011	0.0017
43b	0.5796	0.7323	75b	0.1153	0.1331			
43c	0.2765	0.2765	75c	0.1698	0.1698			
45a	1.9142	2.3940	75d	0.5578	0.7059			
45b	0.381	0.381	75f	0.0289	0.0289			
45c	0.1437	0.1747	76a	0.1475	0.1752			
46a	0.0373	0.0373	76b	0.1432	0.1432			
46b	0.0267	0.0267	76c	0.1524	0.1524			
46c	0.0106	0.0106	76d	0.1483	0.1483			
46d	0.0021	0.0021	76f	0.0740	0.1004			
49a	0.5545	0.8761	82b	0.0505	0.0728			
49b	1.2973	1.7712	82c	0.383	0.383			
49c	0.2576	0.2576	83b	0.048	0.048			
49d	0.1352	0.1352	83c	1.1171	1.3999			
53a	0.6193	0.6194	92c	0.3387	0.5007			
53b	0.06160	0.0616						

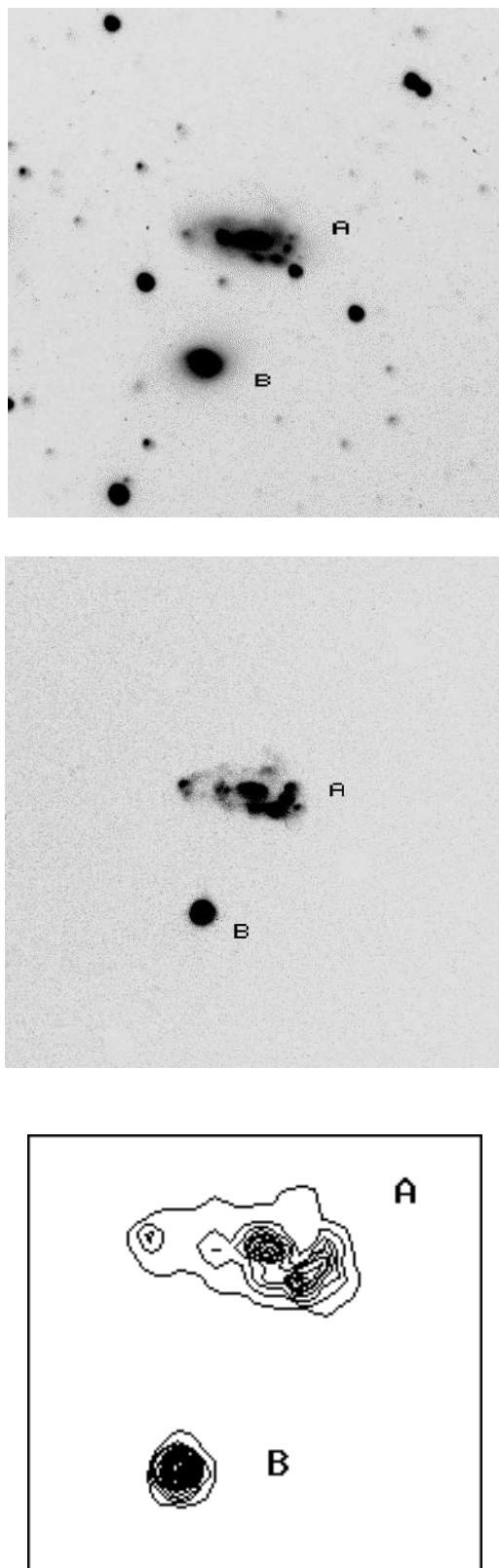


Figure 6: Continuum (up), H_{α} map (middle) and zoomed isocontour map (down) of galaxies A and B of HCG2. The lowest contour is at 1σ ($6.27 \cdot 10^{-17} \text{ erg cm}^2 \text{ s}^{-1} \text{ arcsec}^{-2}$) above the background. The interval among the contours is 3σ .

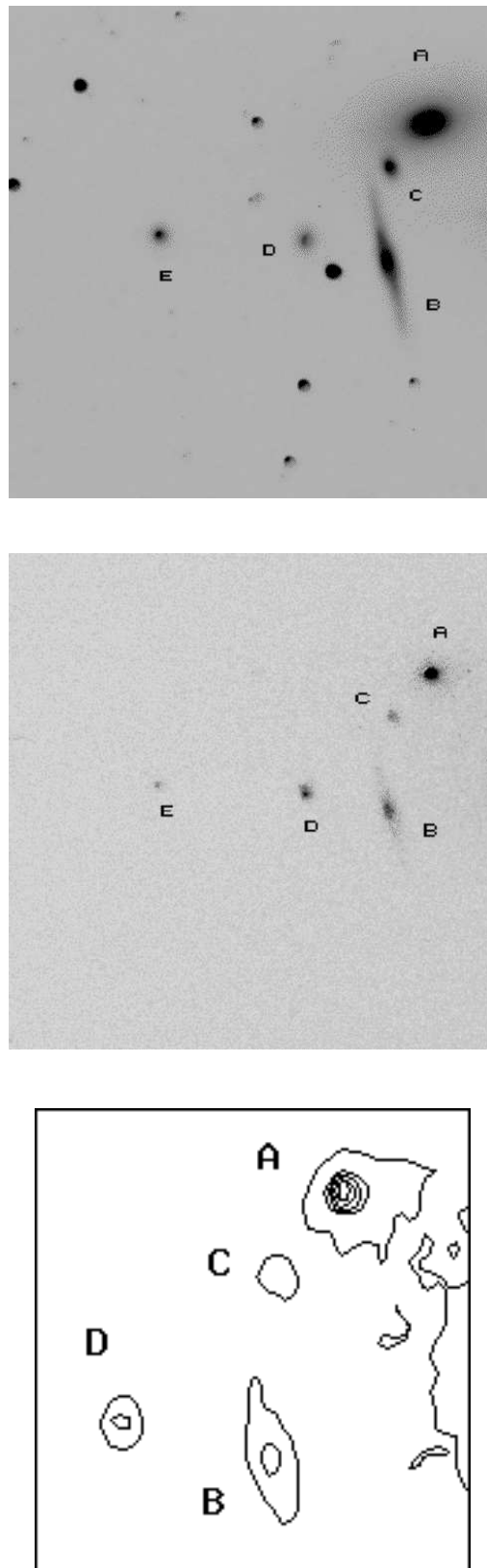


Figure 7: Continuum (up), H_{α} map (middle) and zoomed isocontour map (down) of HCG37. The isocontour plots are given for the largest galaxies only (see Table 7). The lowest contour is at 1σ ($3.64 \cdot 10^{-17} \text{ erg cm}^2 \text{s}^{-1} \text{arcsec}^{-2}$) above the background. The interval among the contours are 3σ .

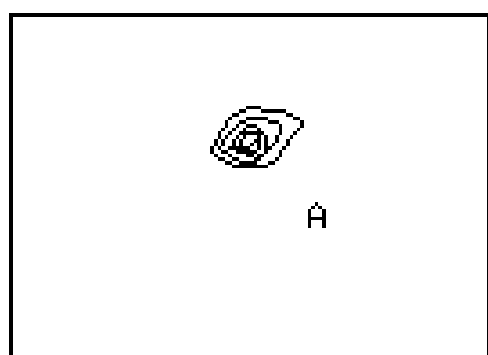
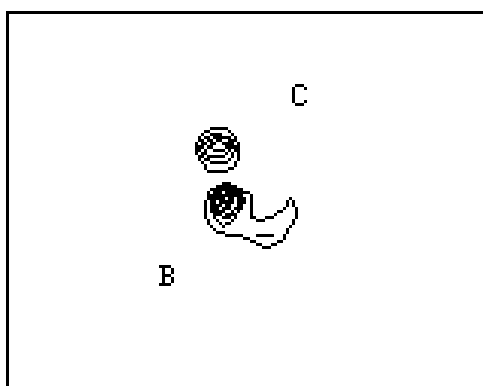
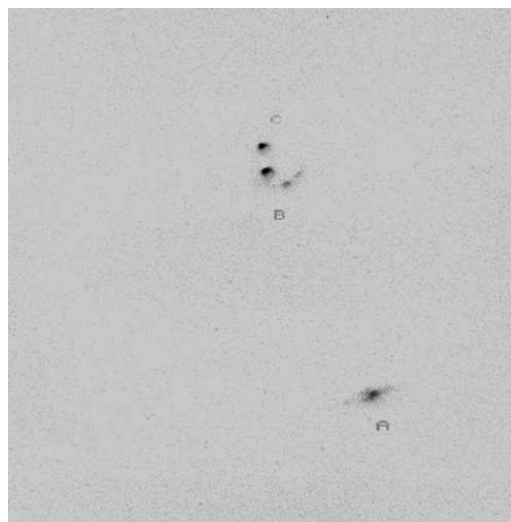
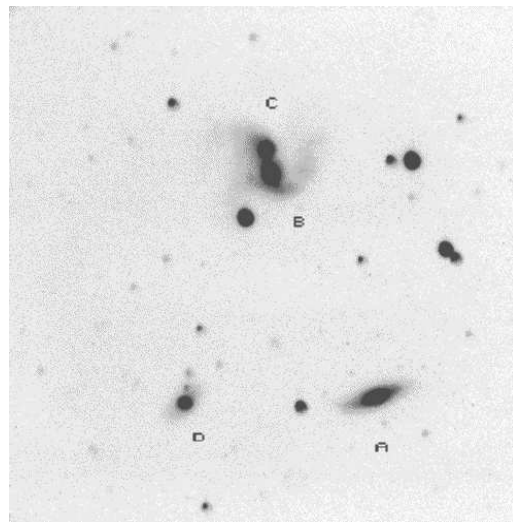


Figure 8: Continuum (up), H_{α} map (middle) and zoomed isocontour map (down) of HCG38. The lowest contour is at 1σ ($7.22 \cdot 10^{-17} \text{ erg cm}^2 \text{s}^{-1} \text{arcsec}^{-2}$) above the background. The interval is 1σ .

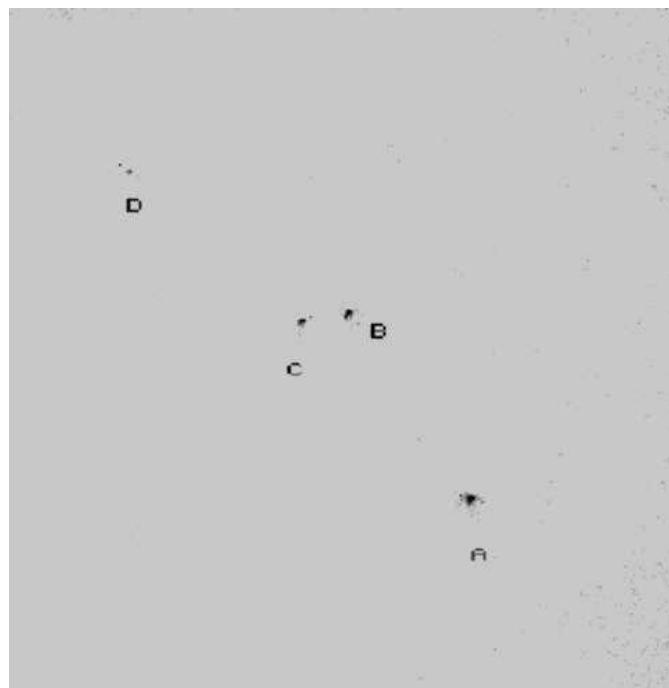
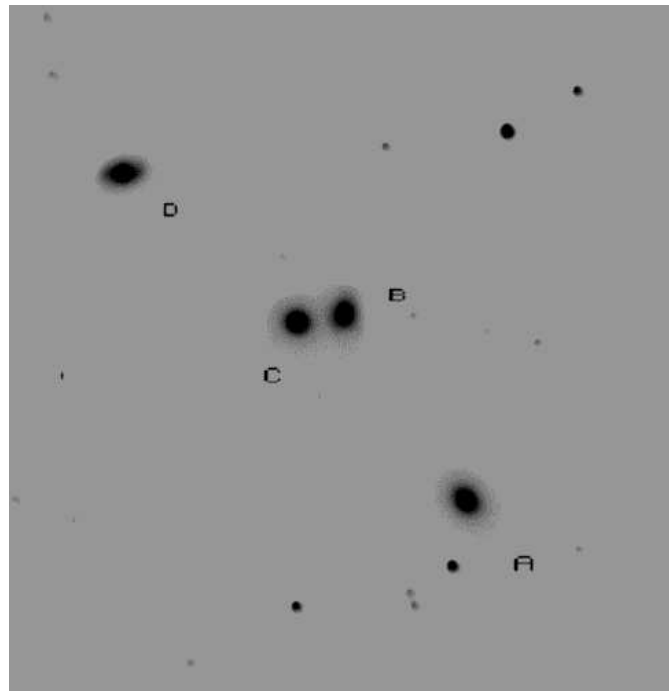


Figure 9: Continuum (up) and H_{α} map (down) of HCG46.

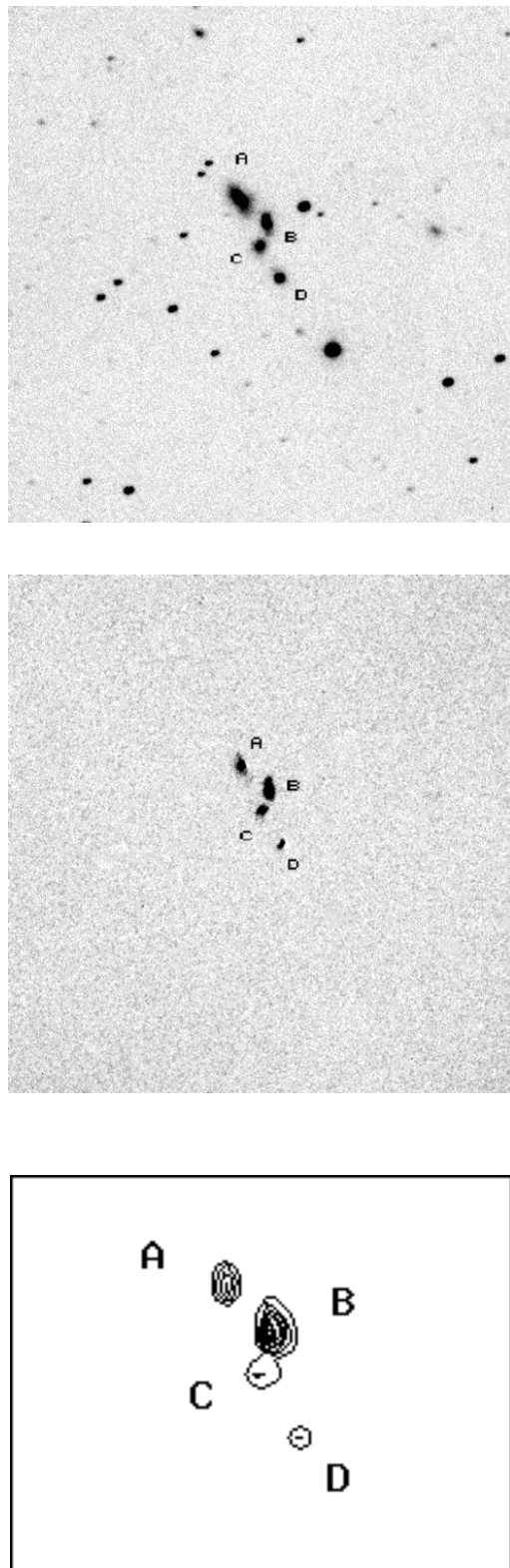


Figure 10: Continuum (up), H_{α} map (middle) and zoomed isocontour map (down) of HCG49. The lowest contour is at 1σ ($9.44 \cdot 10^{-17} \text{ erg cm}^2 \text{s}^{-1} \text{arcsec}^{-2}$) above the background. The interval among the contours is 2σ .

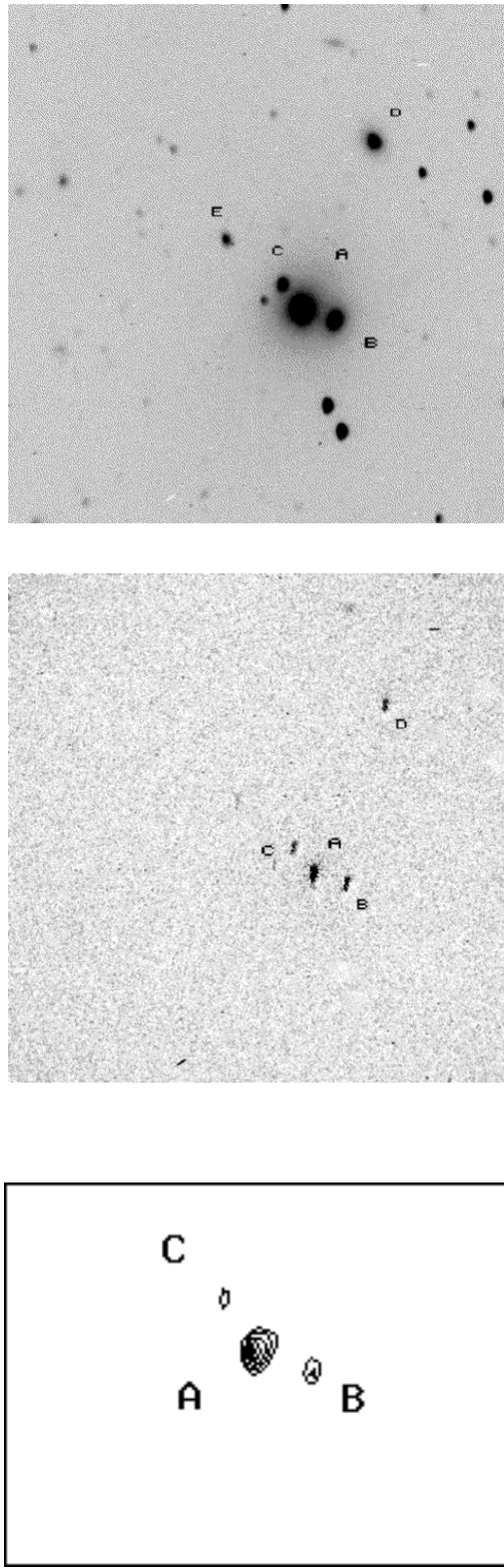


Figure 11: Continuum (up), H_{α} map (middle) and zoomed isocontour map (down) of HCG74. The isocontour plots are given for A, B and C galaxies. The lowest contour is at 1σ ($7.52 \cdot 10^{-17} \text{ erg cm}^2 \text{s}^{-1} \text{arcsec}^{-2}$) above the background. The interval among the contours is 1σ .